Available online at www.sciencedirect.com
SCIENCE DIRECT®
International Journal of Heat and Mass Transfer 47 (2004) 5781–5792
International Journal of HEAT and MASS TRANSFER
www.elsevier.com/locate/ijhmt

# A numerical method for natural convection and heat conduction around and in a horizontal circular pipe

Satoru Yamamoto [a,*], Daisuke Niiyama [a], Byeong Rog Shin [b]

[a] Department of Aeronautics and Space Engineering, Tohoku University, Aobayama 01, Aoba-ku, Sendai 980-8579, Japan
[b] Institute of Fluid Science, Tohoku University, Sendai 980-8577, Japan

Received 1 April 2003; received in revised form 4 April 2004
Available online 6 October 2004

**Abstract**

Natural convection around a horizontal circular pipe coupled with heat conduction in the solid structure is numerically investigated using a preconditioning method for solving incompressible and compressible Navier–Stokes equations. In this method, fundamental equations are completely reduced to an equation of heat conduction when the flow field is static (zero velocity). Therefore, not only compressible flows but also very slow flows such as natural convection in a flow field and heat conduction in a static field can be simultaneously calculated using the same computational algorithm. In this study, we first calculated the compressible flow around a NACA0012 airfoil with conduction in the airfoil and then simulated natural convections around a horizontal circular pipe with a different heat conductivity. Finally, we numerically investigated the effect of heat conductivity of the pipe on natural convection.


*Keywords:* Coupling problem; Natural convection; Heat conduction; Preconditioning method

## 1. Introduction

Natural convection around a horizontal circular cylinder is a classical heat-transfer problem, and many experimental and numerical studies have already been reported. Since the curvature effects and the pressure difference across the laminar boundary-layer formed around the cylinder are negligible at a high Rayleigh number; $Ra > 10^5$, most of the numerical studies assuming this condition have been conducted by solving boundary-layer equations [1,2]. However, Akagi [3], Peterka and Richardson [4], and Gupta and Pop [5] have reported that curvature effects exist for some special cases. Kuehn and Goldstein [6] calculated Navier–Stokes and energy equations for obtaining solutions over a wide range of Rayleigh number; $10^0 \leqslant Ra \leqslant 10^7$. The calculated results corresponded well with the experimental results. In recent studies, natural convections have been numerically investigated by a similar approach as that of the above studies, based on boundary-layer equations or the Boussinesq approximation, even if natural convections are coupled with an additional complicated problem, such as those with enclosure [7] or those with condensation [8].

Natural convection induced by heating with hot vapor or liquid through a circular pipe is also an important problem for power plants to resolve. Cooling is important for electric devices because of micronization. In both cases, heat conduction in the solid phase must be

* Corresponding author. Fax: +81 22 217 6988.
*E-mail address:* yamamoto@caero.mech.tohoku.ac.jp (S. Yamamoto).

0017-9310/$ - see front matter © 2004 Elsevier Ltd. All rights reserved.
doi:10.1016/j.ijheatmasstransfer.2004.06.039

**Nomenclature**

| | | | |
|---|---|---|---|
| $C_p$ | specific heat at constant pressure | $T$ | static temperature |
| $E_i$ | flux-vectors ($i = 1,2$) | $U_i$ | contravariant velocities ($i = 1,2$) |
| $e$ | total internal energy per unit volume | $u_i$ | physical velocities ($i = 1,2$) |
| $F_i$ | flux-vectors in general curvilinear coordinates ($i = 1,2$) | $t$ | time |
| | | $x_i$ | Cartesian coordinates ($i = 1,2$) |
| $H$ | total enthalpy | $\beta$ | preconditioning parameter |
| $J$ | Jacobian of transformation | $\Gamma$ | preconditioning matrix |
| $p$ | static pressure | $\xi_i$ | general curvilinear coordinates ($i = 1,2$) |
| $Q$ | vector of unknown variables in general curvilinear coordinates | $\rho$ | density |
| | | $\mu$ | molecular viscosity |
| $q$ | vector of unknown variables | $\delta_{ij}$ | Kronecker's delta |
| $Re$ | Reynolds number | $\tau_{ij}$ | viscous stress tensors ($i,j = 1,2$) |
| $S$ | vector of diffusion terms | $\kappa$ | heat conductivity |

investigated coupled with the effects of the surrounding flow and natural convection. The numerical study reported by Kuehn and Balvanz [9] may be the first one to present the effect of heat conduction in the solid phase of a pipe on the natural convection around the pipe. This study was extended to a 3-D problem [10]. However, these approaches can apply only to natural convective problems with a simple-shaped solid phase item, such as a circular pipe.

In this study, thermal coupling problems for not only natural convection but also compressible flow around an arbitrary shaped body with the heat conduction in the body are numerically investigated by using a finite-difference algorithm based on compressible flow solvers and the preconditioning method developed by Weiss and Smith [11]. Compressible flow solvers have a certain problem, the so-called stiff problem, when a flow at a very low Mach number is calculated, because convergence of solution cannot be obtained. Therefore, natural convection has not been simulated accurately by the existing compressible flow solvers.

Turkel [12] and Choi and Merkle [13] have proposed a preconditioning method to overcome the stiffness in compressible flow solvers. A numerical speed of sound has been additionally introduced with the pseudo-compressibility into compressible flow solvers as a preconditioning procedure. As a result, fundamental equations are transformed into incompressible Navier–Stokes equations and the temperature equation with pseudo-compressibility only at a very low Mach number. Recently, we developed a preconditioned flux-vector splitting form [14] using a preconditioning approach by Weiss's method [9]. This form has been applied to Roe's approximate Riemann solver [15] and the LU-SGS scheme [16]. The preconditioned method developed by us has already been applied to transonic flows around a NACA0012 airfoil, compressible flows at a very low Mach number, and natural convections in air around a horizontal circular cylinder [14,16]. Since the stiffness problem is completely resolved in the present method, excellent convergence of steady-state solution in all cases could be demonstrated [17]. This method was further applied to a natural convection assuming zero gravity [14,18]. Since there is no gravitational force in the case with zero gravity, convection due to heat-transfer between the cylinder with its constant temperature and the surrounding air could be negligible. This result suggests that our method can be applied in cases of thermal conduction without convection.

In this study, we applied our method to two thermal coupling problems. One was a compressible flow around a NACA0012 airfoil with thermal conduction in the airfoil itself to demonstrate the applicability of the present method to a compressible flow around an arbitrary-shaped body. We also applied the present method to a thermal coupling problem between natural convection and thermal conduction around and in a horizontal circular pipe considering the heat conductivity of the pipe itself. Finally, we numerically investigated the effect of heat conductivity of the pipe on natural convection.

## 2. Numerical methods

### 2.1. Fundamental equations

The fundamental equations used in this study are based on the two-dimensional compressible Navier–Stokes equations. The set of equations is written in vector form as

$$\frac{\partial q}{\partial t} + \frac{\partial E_i}{\partial x_i} + \frac{1}{Re} S = 0 \tag{1}$$

where

$$q = \begin{bmatrix} \rho \\ \rho u_1 \\ \rho u_2 \\ e \end{bmatrix}, \quad E_i = \begin{bmatrix} \rho u_i \\ \rho u_1 u_i + \delta_{i1} p \\ \rho u_2 u_i + \delta_{i2} p \\ (e+p)u_i \end{bmatrix},$$

$$S = -\frac{\partial}{\partial x_i} \begin{bmatrix} 0 \\ \tau_{1i} \\ \tau_{2i} \\ \tau_{ki} u_k + \kappa \partial T / \partial x_i \end{bmatrix} \tag{2}$$

Eq. (1) is further transformed to equations in general curvilinear coordinates. The set of equations is represented by

$$Q_t + L(Q) = \frac{\partial Q}{\partial t} + \frac{\partial F_i}{\partial \xi_i} + \frac{1}{Re} S = 0 \tag{3}$$

where

$$Q = Jq, \quad F_i = J(\partial \xi_i / \partial x_j) E_j, \quad J = \partial(x_1 x_2)/\partial(\xi_1 \xi_2) \tag{4}$$

The stress tensor $\tau_{ij}$ is given by

$$\tau_{ij} = \mu \left[ \left( \frac{\partial u_i}{\partial x_j} + \frac{\partial u_j}{\partial x_i} \right) - \frac{2}{3} \delta_{ij} \frac{\partial u_k}{\partial x_k} \right] \tag{5}$$

and natural convections calculated in this study are assumed to be laminar convection.

Many numerical studies for simulating natural convections have been reported in the last several decades. In most of the studies, incompressible Navier–Stokes equations with the Bussinesq assumption have been solved. Natural convections are induced by the buoyancy effect with the small density change of a working gas or liquid and hence are an exactly compressible flow. However, ordinary compressible flow solvers could not be applied to the calculation. One of the reasons is the so-called stiff problem that occurs when flows at a very low Mach number are calculated by compressible flow solvers. The relatively high speed of sound compared with physical velocities in these flows restricts the Courant–Friedrich–Lewy (CFL) number. Then, we need a huge number of time-marching iterations to get a solution.

Recently, Turkel [12], Choi and Merkle [13], and Weiss and Smith [11] have developed a preconditioning method that is a numerical approach to overcoming the stiff problem. A numerical speed of sound has been derived and applied to the pseudo-compressibility method. Fundamental equations are smoothly switched to different equations according to the value of the numerical speed of sound. The equations are completely the same with the compressible Navier–Stokes equations when the value is set to the physical speed of sound, while the incompressible Navier–Stokes equations with the pseudo-compressibility term and the temperature equation are formed by setting the value to that in a same order of local physical velocity. Natural convective problems have already been calculated using the preconditioning method [13], and we have employed the same approach in this study.

The fundamental equations modified by the preconditioning method are written in general curvilinear coordinates as

$$\Gamma \widehat{Q}_t + L(\widehat{Q}) = \Gamma \frac{\partial \widehat{Q}}{\partial t} + \frac{\partial F_i}{\partial \xi_i} + \frac{1}{Re} S = 0 \tag{6}$$

where $\Gamma$ is the preconditioning matrix. The elements in $\Gamma$ are fundamentally the same as those of the formulation by Weiss and Smith [11], represented as

$$\Gamma = \begin{bmatrix} \beta & 0 & 0 & \rho_T \\ \beta u_1 & \rho & 0 & \rho_T u_1 \\ \beta u_2 & 0 & \rho & \rho_T u_2 \\ \beta H - 1 & \rho u_1 & \rho u_2 & \rho_T H + \rho C_p \end{bmatrix} \tag{7}$$

where $\beta$ is the preconditioning parameter, which is defined by

$$\beta = 1/U_r^2 - \rho_T / \rho C_p \tag{8}$$

and $\rho_T = \partial \rho / \partial T$. Since only ideal gas is taken into consideration in this study, $\rho_T = -\rho/T$. $U_r$ is a switching parameter. If $U_r$ equals the physical speed of sound, $\beta$ is to be zero and the fundamental equations are reduced to the compressible Navier–Stokes equations. $\widehat{Q}$ is the vector of unknown primitive variables defined by $\widehat{Q} = [p \quad u_1 \quad u_2 \quad T]^{\mathrm{T}}$.

### 2.2. Preconditioned flux-vector splitting form

Eq. (6) has been solved by a finite-difference or finite-volume method based on compressible flow solvers such as approximate Riemann solvers. We have developed a high-resolution finite-difference method for simulating unsteady transonic viscous flows. In this method, we employed the fourth-order compact MUSCL TVD (Compact MUSCL) scheme [19], Roe's approximate Riemann solver [15], and the LU-SGS scheme [16]. In a previous study, a preconditioned flux-vector splitting (PFVS) form for inviscid terms was newly derived and applied to the high-resolution method [14]. Then, a preconditioned Roe's scheme and a preconditioned LU-SGS scheme were introduced by using the splitting form. The PFVS form is briefly explained below.

The numerical flux $(F_i)_{\ell+1/2}$ for $F_i$ in Eq. (6) defined at the interface between the control volume $\ell$ and $\ell+1$ in each coordinate $i$ ($i = 1, 2$) can be written by a flux-vector splitting form as

$$\begin{aligned} (F_i)_{\ell+1/2} &= \left(F_i^+\right)_{\ell+1/2} + \left(F_i^-\right)_{\ell+1/2} \\ &= \left(\widehat{A}_i^+\right)_{\ell+1/2} \widehat{Q}^L_{\ell+1/2} + \left(\widehat{A}_i^-\right)_{\ell+1/2} \widehat{Q}^R_{\ell+1/2} \end{aligned} \tag{9}$$

The superscripts $\mp$ indicate the sign of characteristic speeds. $F_i^{\mp}$ are the numerical flux-vectors composed of only positive or negative characteristic speeds. $\widehat{A}_i^{\mp}$ are the preconditioned Jacobian matrices composed of only positive or negative characteristic speeds. $\widehat{Q}^L$ and $\widehat{Q}^R$ are the unknown vectors extrapolated by the compact MUSCL [19] from left and right directions. The preconditioned flux-vector splitting form for $(\widehat{A}_i^{\mp})_{\ell+1/2}\widehat{Q}^M_{\ell+1/2}$ derived in the previous study is given by

$$\left(\widehat{A}_i^{\mp}\right)_{\ell+1/2}\widehat{Q}^M = \left(\Gamma L_i^{-1}\Lambda_i L_i\right)_{\ell+1/2}\widehat{Q}^M = \hat{\lambda}_{i1}^{\mp}\Gamma\widehat{Q}^M + \frac{\hat{\lambda}_{ia}^{\mp}}{\hat{c}_i\sqrt{g_{ii}}}\widehat{Q}_{ia} + \frac{\hat{\lambda}_{ib}^{\mp}}{\hat{c}_i^2}\widehat{Q}_{ib} \tag{10}$$

The superscript $M$ is replaced by $L$ or $R$. $g_{ii} = \nabla\xi_i\cdot\nabla\xi_i$. $L_i$ and $\Lambda_i$ are the matrices composed of preconditioned eigenvectors and preconditioned characteristic speeds (eigenvalues). $\hat{\lambda}_{ia}^{\mp}$ and $\hat{\lambda}_{ib}^{\mp}$ are defined by

$$\hat{\lambda}_{ia}^{\mp} = \left(\hat{\lambda}_{i3}^{\mp} - \hat{\lambda}_{i4}^{\mp}\right)/2 \tag{11}$$

$$\hat{\lambda}_{ib}^{\mp} = \left(\ell_i^{-}\hat{\lambda}_{i3}^{\mp} - \ell_i^{+}\hat{\lambda}_{i4}^{\mp}\right)/\left(\ell_i^{-} - \ell_i^{+}\right) - \hat{\lambda}_{i1}^{\mp} \tag{12}$$

where $\hat{\lambda}_{ij}^{\mp}$ $(j = 1,3,4)$ and $\ell_i^{\mp}$ are calculated by

$$\hat{\lambda}_{ij}^{\mp} = \left(\hat{\lambda}_{ij} \pm |\hat{\lambda}_{ij}|\right)/2 \tag{13}$$

$$\ell_i^{\mp} = \rho U_r^2/\left(U_i(1-\alpha)/2 \mp \hat{c}_i\sqrt{g_{ii}}\right) \tag{14}$$

$\hat{\lambda}_{ij}$ $(j = 1,3,4)$ are the preconditioned characteristic speeds derived as

$$\hat{\lambda}_{i1} = U_i \tag{15}$$

$$\hat{\lambda}_{i3} = (1+\alpha)U_i/2 + \hat{c}_i\sqrt{g_{ii}} \tag{16}$$

$$\lambda_{i4} = (1+\alpha)U_i/2 - \hat{c}_i\sqrt{g_{ii}} \tag{17}$$

In Eqs. (14), (16), and (17), $\hat{c}_i$ is the numerical speed of sound. It is defined by

$$\hat{c}_i = \sqrt{U_i^2(1-\alpha)^2/g_{ii} + 4U_r^2}\Big/2 \tag{18}$$

and $\alpha = U_r^2(\rho_p + \rho_T/\rho C_p)$, where $\rho_p = \partial\rho/\partial p$. In this study, $\rho_p = 1/(RT)$ for ideal gas. $R$ is the gas constant. If $U_r$ equals the physical speed of sound, $\alpha$ is reduced to unit. Then, characteristic speeds and the physical speed of sound for compressible flows are recovered in Eqs. (16) and (17). $\widehat{Q}_{ia}$ and $\widehat{Q}_{ib}$ are the subvectors defined by

$$\hat{Q}_{ia} = \hat{q}_1^M Q_{ic} + \rho\widehat{U}_i Q_d \tag{19}$$

$$\hat{Q}_{ib} = (\rho\widehat{U}_i\hat{c}_i^2/g_{ii})Q_{ic} + (\hat{q}_1^M\hat{c}_i^2/U_r^2)Q_d \tag{20}$$

$\hat{q}_j^M$ and $\widehat{U}_i[= (\partial\xi_i/\partial x_j)\hat{q}_{j+1}^M (j = 1,2)]$ are the $j$th element of $\hat{Q}$ and the contravariant velocities extrapolated by the compact MUSCL [19] in which $M = L$ or $R$, respectively. $Q_{ic}$ and $Q_d$ are the subvectors given by

$$Q_{ic} = [\,0 \quad \partial\xi_i/\partial x_1 \quad \partial\xi_i/\partial x_2 \quad U_i\,]^{\mathrm{T}} \tag{21}$$

$$Q_d = [\,1 \quad u_1 \quad u_2 \quad (e+p)/\rho\,]^{\mathrm{T}} \tag{22}$$

### 2.3. Preconditioned Roe's scheme

In this study, the flux-difference splitting method based on Roe's approximate Riemann solver [15] is used for the space difference. This method can be easily modified by employing the preconditioned flux-vector splitting form in Eq. (10). The numerical flux in Eq. (9) can be alternatively defined by Roe's algorithm as

$$(F_i)_{\ell+1/2} = \frac{1}{2}[F_i(\hat{Q}^L_{\ell+1/2}) + F_i(\hat{Q}^R_{\ell+1/2}) - |(\hat{A}_i)_{\ell+1/2}|(\hat{Q}^R_{\ell+1/2} - \hat{Q}^L_{\ell+1/2})] \tag{23}$$

The numerical flux of the flux-difference splitting term in Eq. (23) is replaced by the following equation simply modified from Eq. (10):

$$|(\hat{A}_i)_{\ell+1/2}|\hat{Q}^M = |\hat{\lambda}_{i1}|\Gamma\hat{Q}^M + \frac{|\hat{\lambda}_{ia}|}{\hat{c}_i\sqrt{g_{ii}}}\hat{Q}_{ia} + \frac{|\hat{\lambda}_{ib}|}{\hat{c}_i^2}\hat{Q}_{ib} \tag{24}$$

All components in Eq. (24) are the same as those in Eq. (10).

### 2.4. Preconditioned LU-SGS scheme

The lower–upper symmetric Gauss–Seidel (LU-SGS) scheme [16] is modified to the preconditioned scheme for time integration. The preconditioned LU-SGS can be defined by the following two equations:

$$\Gamma D\Delta\hat{Q}^* = RHS + \Delta t G^+(\Delta\hat{Q}^*) \tag{25}$$

$$\Delta\hat{Q} = \Delta\hat{Q}^* - \Gamma^{-1}D^{-1}\Delta t G^-(\Delta\hat{Q}) \tag{26}$$

where $RHS$ is the vector of explicit time-marching residues of Eq. (6). $\Delta t$ is the time step. $D$ is the diagonal matrix approximated by the spectral radius of the preconditioned Jacobian matrices. $G^+$ and $G^-$ are functions composed of time derivatives of numerical flux at neighboring grid points defined by

$$G^+(\Delta\widehat{Q}^*) = (\widehat{A}_1^+\Delta\widehat{Q}^*)_{i-1,j} + (\widehat{A}_2^+\Delta\widehat{Q}^*)_{i,j-1} \tag{27}$$

$$G^-(\Delta\widehat{Q}) = (\widehat{A}_1^-\Delta\widehat{Q})_{i+1,j} + (\widehat{A}_2^-\Delta\widehat{Q})_{i,j+1} \tag{28}$$

The lower scripts $i$, $j$ indicate a grid point where the time derivatives of numerical flux are located. In our approach, these time derivatives on the right-hand side of Eqs. (27) and (28) are calculated by using the preconditioned flux-splitting form of Eq. (10). Then, $\widehat{Q}^M$ in Eq. (10) has only to be replaced by $\Delta\widehat{Q}$.

## 3. Heat conduction in a solid

Heat conduction in a static field is governed by a parabolic partial-differential equation. In two-dimensions, it is defined by

$$\frac{\partial T}{\partial t} = \kappa\left(\frac{\partial^2 T}{\partial x^2} + \frac{\partial^2 T}{\partial y^2}\right) \tag{29}$$

In the preconditioning approach, the fundamental equations are transformed to incompressible Navier–Stokes equations with a pseudo-compressibility term and the temperature equation when local velocity is very low. An extreme case is when whole velocities are zero. In this condition, all terms including velocity components are neglected from Eq. (1), and the pressure derivative can be omitted if it assumes no pressure waves in the static field. Finally, Eq. (1) is reduced to only the same equation with Eq. (29). Other equations are disappeared. Therefore, static fields in liquid and solids can be calculated using the present method by setting zero velocities and different heat conductivities.

One simple problem for heat conduction in a rectangular field is calculated to validate the accuracy of the present method. Fig. 1 shows the schematic of boundary conditions. The left and top faces are heated to 373 [K], and the temperature of the right and bottom faces is fixed at 273 [K]. The calculated result using the present method is compared with that calculated by Eq. (29) using the Crank–Nicolson and SOR relaxation method. Fig. 2(a) and (b) show the calculated results by the present method and the relaxation method. We also compared the local values of temperature in Fig. 2(a) and (b) at several points and found that they matched within second-order accuracy in space, which indicates that the present set of equations can be reduced to the equation of heat conduction of Eq. (29).

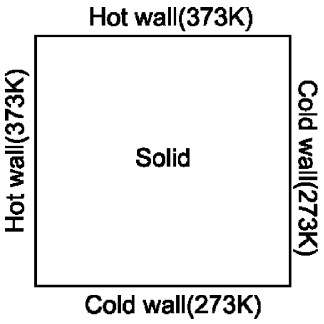


Fig. 1. Schematic of boundary conditions.

## 4. Results

### 4.1. Natural convection around a horizontal circular cylinder

We calculated the natural convections around a horizontal circular cylinder reported by Kuehn and Goldstein [6] to check the reliability of the present method. As flow conditions, the uniform temperature far from the cylinder was 293 [K], and the surface temperature on the cylinder was 325.5 [K]. The temperature in the cylinder was also fixed at 325.5 [K]. The working gas was dry air, and we used an O-type grid with $181 \times 45$ grid points. The gravitational force was added in the source term for the momentum and energy equations. The Rayleigh number was fixed at $Ra = 10^5$.

Fig. 3 shows the calculated temperature contours (left hand side) compared with the experimental fringe pattern (right hand side) reported in Kuehn and Goldstein [6]. The dry air was heated on the cylinder surface, and then heat convection occurred around the cylinder and the heated air moved upward due to the buoyancy effect. The calculated pattern is quite in good agreement with the result of experiment [6].

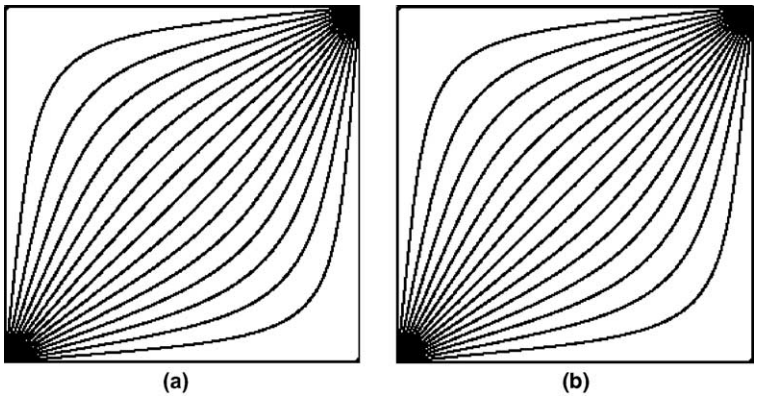


Fig. 2. Temperature contours: (a) present method, (b) solution from the heat conductivity equation.

Fig. 3. Calculated temperature contours (left hand side) and the experimental fringe pattern (right hand side, Kuehn and Goldstein [6]) around horizontal circular cylinder at $Ra = 10^5$.

Fig. 4 shows the calculated non-dimensional temperature distributions on normal lines from the cylinder surface at $\theta = 90°$ and 180°, where $\theta$ is the angle around the cylinder from the bottom normal line. $\phi$ is a temperature ratio defined by $(T - T_\infty)/(T_w - T_\infty)$, where $T_\infty$ is the uniform temperature far from the cylinder surface and $T_w$ is the temperature at the cylinder surface. $Y^*$ is the distance from the cylinder surface defined by $R_a^{\frac{1}{4}} Y/D$, where $D$ is the diameter of the cylinder. The calculated temperatures are in good agreement with the results of the experiments.

Fig. 5 shows the calculated Nusselt number distributions around the cylinder. The calculated results are also in good agreement with the those of the experiments. From these comparisons with the experiments, we were able to assess the reliability of the present method applied to the problem of natural convections around the cylinder.

Next, we calculated natural convections in the same flow conditions except for the Rayleigh number. The Rayleigh number is changed by varying only the diameter of the circular cylinder. Fig. 6(a)–(d) show the calculated temperature contours at $Ra = 1, 10^2$, $10^4$, and $10^6$. The value of temperature from 293 [K] to 325.5 [K] is divided by sixteen contour lines. These results are in good agreement with those of the calculation by Kuehn and Goldstein [6]. The thermal boundary-layer is very thick in the case of $Ra = 1$ because the diameter of the circular cylinder is very small. The width of the thermal boundary-layer is considerably larger than the diameter. According to the increase in Rayleigh number, the thickness of the thermal boundary layer is decreased. Especially, the thinnest thermal boundary-layer is observed in the case of $Ra = 10^6$. A thin thermal plume is also formed upon the cylinder.

### 4.2. Compressible flow around a NACA0012 airfoil with thermal conduction in the airfoil

A unique point of our numerical approach may be its applicability to a wide range of thermal coupling problems such as not only that between natural convection and thermal conduction around and in a circular pipe, but also compressible flows around an arbitrary-shaped body with thermal conduction in the body. Although the main purpose of this report is to show the calculated

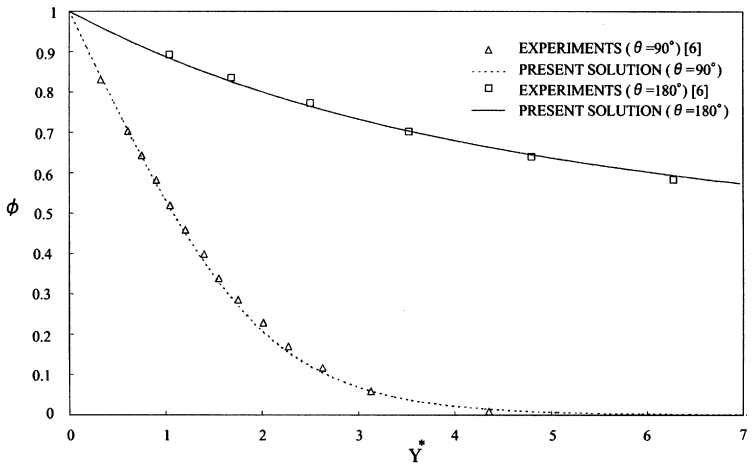


Fig. 4. Temperature distributions at $\theta = 90°$ and 180°.

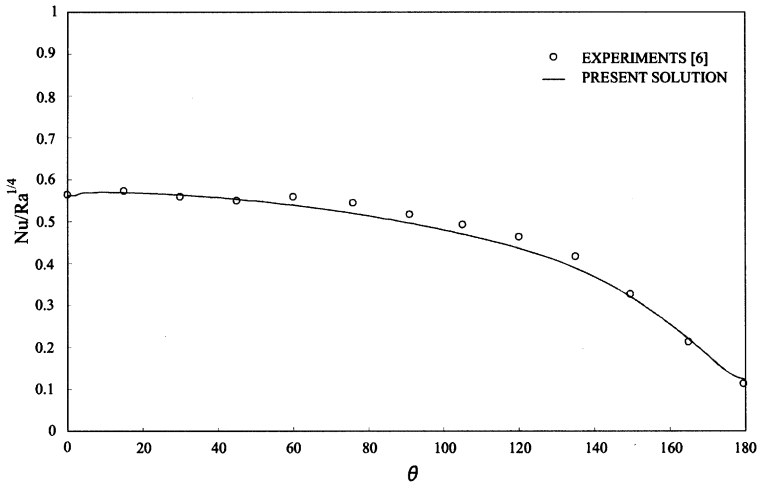


Fig. 5. Nusselt number distributions around the cylinder.

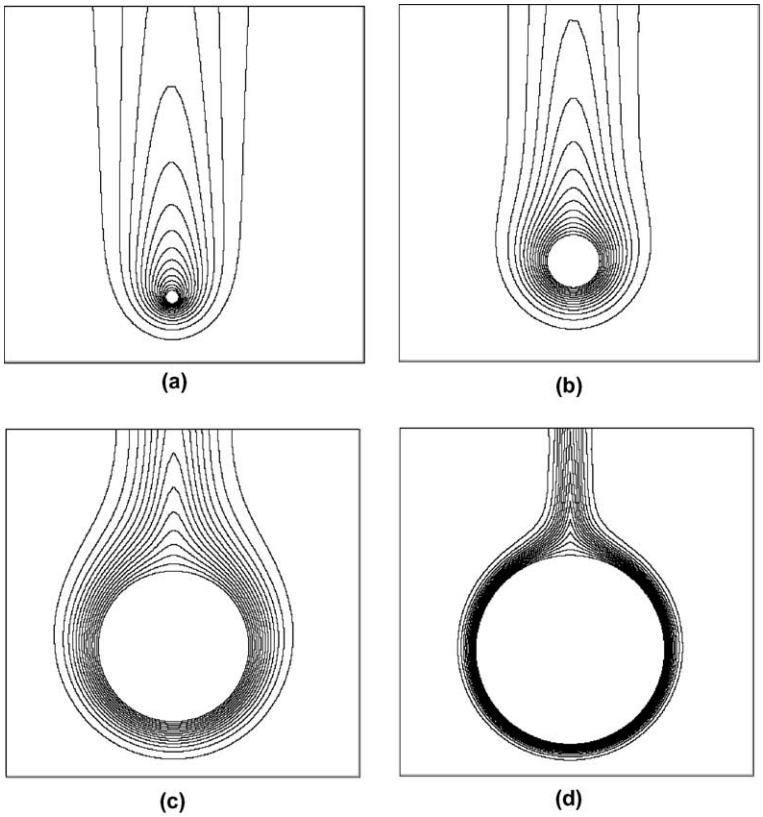


Fig. 6. Temperature contours around the cylinder: (a) $Ra = 1$, (b) $Ra = 10^2$, (c) $Ra = 10^4$, (d) $Ra = 10^6$.

results of natural convection and heat conduction in and around a horizontal and circular pipe, we also calculated the compressible flow around a NACA0012 airfoil with thermal conduction in the airfoil and include the calculated results here to demonstrate the applicability of the present method.

Fig. 7(a) shows the schematic of the present problem. The airfoil has a skin with a finite thickness in the body.

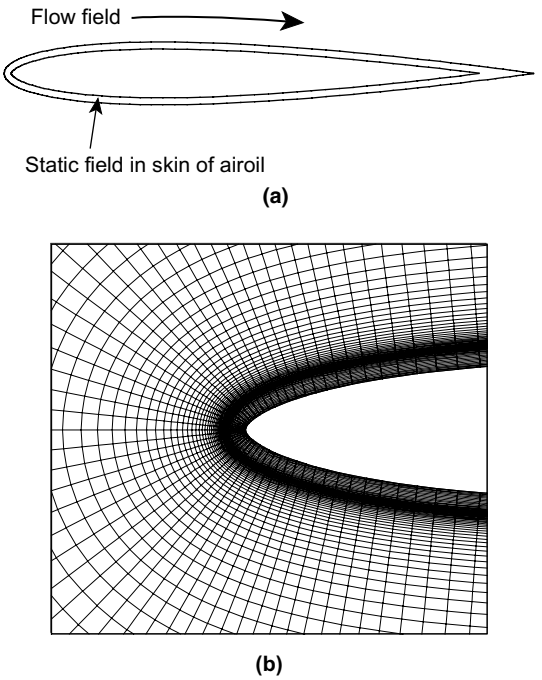


Fig. 7. (a) Schematic of the skin of NACA0012 airfoil. (b) Computational grid focused on the leading edge.

The flow conditions are that the uniform Mach number was 0.1, the uniform temperature was 293 [K], and the Reynolds number was $3.4 \times 10^6$. The heat conductivity of the skin was set at $5\kappa$, where $\kappa$ is the heat conductivity of dry air. The temperature at the inner side of the skin was fixed at 294 [K]. Of course, this temperature can be increased or decreased. We set up this value to be able to draw temperature contours both in the skin and in the flow field. We used a C-type grid with $221 \times 93$ grid points around the airfoil and $221 \times 24$ grid points in the skin. Fig. 7(b) shows the computational grid near the leading edge.

Fig. 8(a) and (b) show the calculated Mach number contours around the airfoil and the focused figure on the leading edge. A compressible flow was successfully calculated by using the present method.

Fig. 9(a) shows the calculated temperature contours around the airfoil and in the skin, and the focused figure on the leading edge is shown in Fig. 9(b). We found that the skin has a temperature gradient between the temperature of the inner side of the skin and that on the airfoil surface. This result indicates that temperature in the skin is influenced by the flow temperature around the airfoil. Although we unfortunately have no experimental data for this problem, the applicability of the present method to a compressible flow around an arbitrary-shaped body with conduction in the body itself can be remarked. In the following section, we apply the present method to the main problem in this study.

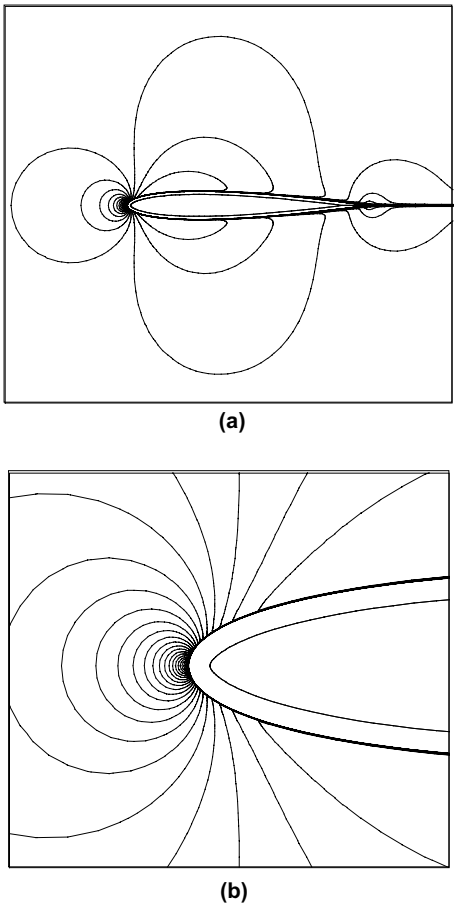


Fig. 8. Mach number contours: (a) in flow field, (b) focused on the leading edge.

### 4.3. Natural convection and heat conduction around and in a horizontal circular pipe

Natural convection induced by the heating from hot vapor or liquid through a circular pipe is an important problem that power plants must resolve. Heat conduction in the solid phase must be investigated coupled with the surrounding flow and natural convection. In this study, a simplified problem is numerically investigated using the method described above. The model considered here is schematically summarized in Fig. 10. The fundamental flow conditions in this test are the same as those listed in Section 4.1. The reference Rayleigh number is $10^5$. The inner wall of the pipe is constantly heated at 325.5 [K], which is the same temperature as the surface temperature of the cylinder in the previous case. Here we assume that the inner channel of the pipe is to be filled with uniformly hot liquid. Three different heat conductivities of the pipe; $5\kappa$, $10\kappa$, and $20\kappa$, are taken into account, where $\kappa$ is the heat conductivity of dry air.

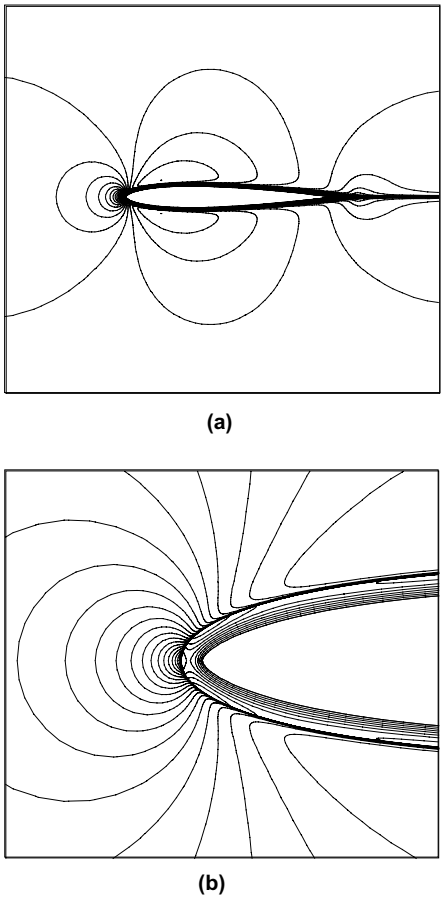


Fig. 9. Temperature contours: (a) in flow field and in the skin, (b) focused on the leading edge.

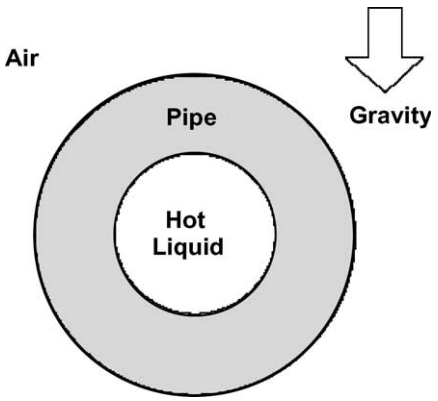


Fig. 10. Schematic of the horizontal circular pipe.

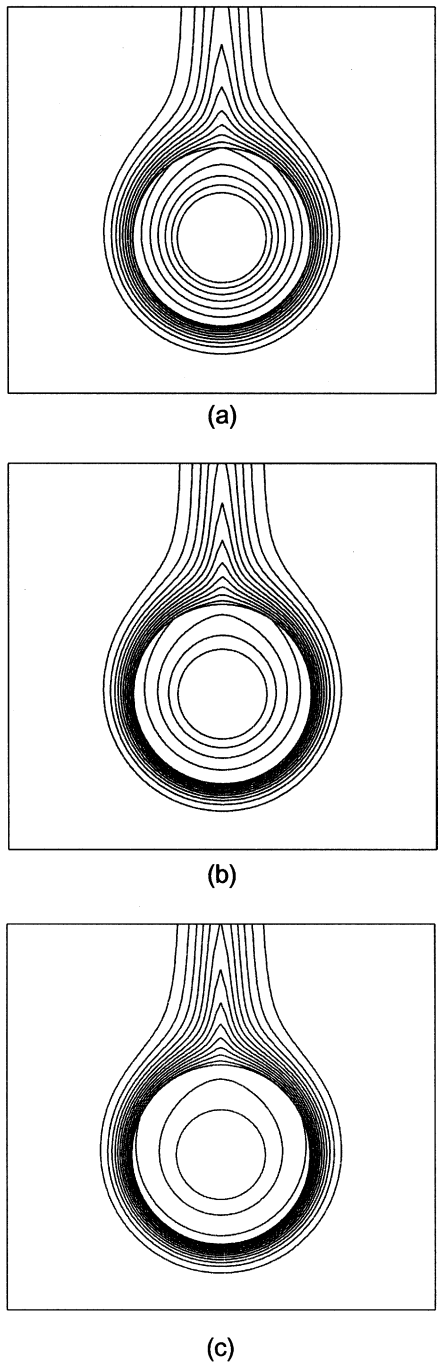


Fig. 11. Temperature contours around and in the pipe: (a) $K = 5\kappa$, (b) $K = 10\kappa$, (c) $K = 20\kappa$.

Fig. 11(a)–(c) show the calculated temperature contours around the pipe and in the body of the pipe. The temperature values are divided by sixteen contour lines as was seen in Fig. 6. In all cases, the surrounding air around the pipe is heated, and a thermal boundary-layer and a thermal plume are formed. On the other hand, temperature distributions are observed between the

inner wall and the outer surface of the pipe in every case. Temperature contours around and in the pipe are connected at the pipe surface. The upper face of the pipe tends to be more heated than the other region, because of heat released from the pipe due to convection. The thermal energy in the body of the pipe is transferred to the surrounding air through the pipe surface. Since the buoyancy effect induces a thermal plume upon the pipe, larger convection in the plume provides higher heat removal from the pipe. The effects of the difference of temperature distributions on heat conductivity of the pipe are explicitly compared in Fig. 11. These figures show the obvious fact that higher heat conduction occurs when a higher heat conductivity of the pipe is specified.

Fig. 12 shows the calculated temperature distributions on normal lines from the pipe surface at $\theta = 90°$ and 180° for the three cases compared with the calculated results in Fig. 4. Since the temperature on the pipe surface decreases according to the decrease in heat conductivity of the pipe, as shown in Fig. 11, the temperature distributions on the normal lines are also influenced by the temperature on the pipe surface.

Fig. 13 shows the calculated Nusselt number around the pipe for the three cases compared with the calculated results in Fig. 5. The inner wall temperature of the pipe; $T_w = 325.5$ [K], is specified for the reference wall temperature to define the Nusselt number in all cases. Nusselt number distributions are also influenced by the temperature difference on the pipe surface. A lower temperature

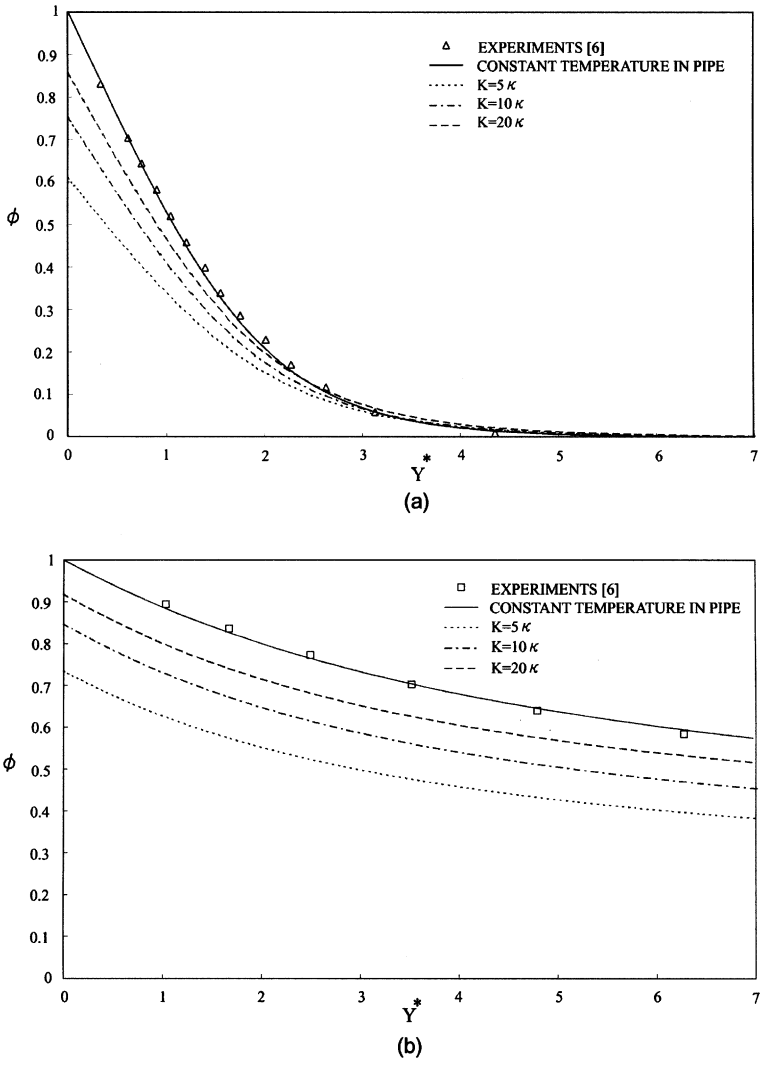


Fig. 12. Temperature distributions at $\theta = 90°$ and 180°: (a) $\theta = 90°$, (b) $\theta = 180°$.

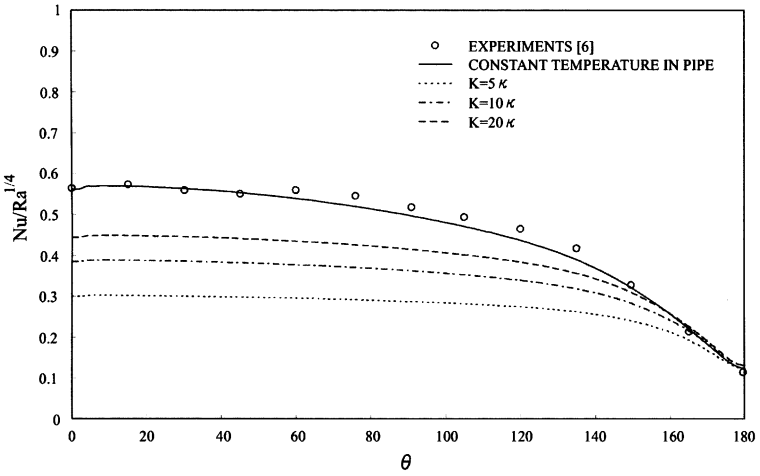


Fig. 13. Nusselt number distributions around the pipe.

on the pipe surface due to lower heat conductivity of the pipe results in a lower Nusselt number. We noted that the slight drop in the Nusselt number at $\theta = 0°$ found in Fig. 13 may be a trivial numerical error due to the treatment of the boundary condition close to this degree.

## 5. Concluding remarks

A numerical method based on the preconditioning method has been applied to the calculation of natural convection and heat conduction around and in a horizontal circular pipe. Natural convections around the pipe with constant temperature were calculated to check the reliability of the present method. The calculated thermal boundary-layers and the Nusselt number around the pipe were in good agreement with the experimental results. Heat conduction in the body of the pipe was additionally taken into account with the calculation of the natural convection around the pipe. Then, the heat flux in the pipe could be successfully calculated by using the same computational algorithm with the natural convection. Lower heat conductivity of the pipe resulted in lower temperature on the surface of the pipe. Since a thermal plume that forms upon the pipe due to the buoyancy effect induces a higher heat release from the upper side of the pipe, temperature at the upper region of the pipe was relatively increased compared with that at other regions.

Finally, as indicated by the results of the coupling problem for a NACA0012 airfoil described in Section 4.2, we conclude that the present method can be also applied to a coupling problem, such as natural convection and heat conduction around and in an arbitrary-shaped body. We will calculate this problem if any experimental data could be provided in future.

## Acknowledgments

The authors wish to acknowledge that this study was carried out as a part of the "Ground-based Research Announcement for Space Utilization" promoted by the Japan Space Forum. In addition, this study was partly supported by the Grant-in-Aid for Scientific Research C no. 12650154 promoted by JSPS.

## References

[1] S. Levy, Integral methods in natural convection flow, J. Appl. Mech. 22 (1955) 515–522.
[2] D.A. Saville, S.W. Churchill, Laminar free convection in boundary layers near horizontal cylinders and vertical axisymmetric bodies, J. Fluid Mech. 29 (1967) 391–399.
[3] S. Akagi, The effect of curvature on free convection from a horizontal cylinder, Trans. JSME 31 (1965) 1327–1335.
[4] J.A. Peterka, P.D. Richardson, Natural convection from a horizontal cylinder at moderate Grashof numbers, Int. J. Heat Mass Transfer 12 (1969) 749–752.
[5] A.S. Gupta, I. Pop, Effects of curvature on unsteady free convection past a circular cylinder, Phys. Fluids 20 (1977) 162–163.
[6] T.H. Kuehn, R.J. Goldstein, Numerical solution to the Navier–Stokes equations for laminar natural convection about a horizontal isothermal circular cylinder, Int. J. Heat Mass Transfer 23 (1980) 971–979.
[7] N.K. Ghaddar, Natural convection heat transfer between a uniformly heated cylindrical element and its rectangular enclosure, Int. J. Heat Mass Transfer 35 (1992) 2327–2334.
[8] M. Mosaad, Combined free and forced convection laminar film condensation on an inclined circular tube with isothermal surface, Int. J. Heat Mass Transfer 42 (1999) 4017–4025.

[9] T.H. Kuehn, J.L. Balvanz, Conjugate heat transfer by natural convection from a horizontal heat exchanger tube, in: Proc. 7th Int. Heat Transfer Conf., vol. 2, 1982, p. 317.
[10] A.K. Tolpadi, T.H. Kuehn, Computation of conjugate 3-dimensional natural-convection heat-transfer from a transversely finned horizontal cylinder, Numer. Heat Transfer 16 (1989) 1.
[11] J.M. Weiss, W.A. Smith, Preconditioning applied to variable and constant density flows, AIAA J. 33 (1995) 2050–2057.
[12] E. Turkel, Preconditioned methods for solving the incompressible and low speed compressible equations, J. Comput. Phys. 72 (1987) 277–298.
[13] Y.-H. Choi, C.L. Merkle, The application of preconditioning in viscous flows, J. Comput. Phys. 105 (1993) 207–223.
[14] S. Yamamoto, B.-R. Shin, Preconditioned implicit flux-splitting scheme for condensate flows, in: Proc. of 2nd Int. Conf. on Computational Fluid Dynamics—Sydney, Springer, 2002, pp. 112–117.
[15] P.L. Roe, Approximate Riemann solvers, parameter vectors, and difference schemes, J. Comput. Phys. 43 (1981) 357–372.
[16] S. Yoon, A. Jameson, Lower–upper symmetric-Gauss–Seidel method for the Euler and Navier–Stokes equations, AIAA J. 26 (1988) 1025–1026.
[17] S. Yamamoto, D. Niiyama, B.R. Shin, Preconditioning implicit flux-splitting scheme and its application to thermal-fluid convections, Trans. JSME, Ser. B 69 (2003) 274–279 (in Japanese).
[18] S. Yamamoto, D. Niiyama, B.R. Shin, Preconditioning high-resolution scheme for gravitational flows with condensation, in: Proc. of 4th ASME-JSME Joint Fluids Engineering Conference, Honolulu, FEDSM2003-45390, 2003.
[19] S. Yamamoto, H. Daiguji, Higher-order-accurate upwind schemes for solving the compressible Euler and Navier–Stokes equations, Comput. Fluids 22 (1993) 259–270.